Chin. J. Mech. Eng. (2017) 30:951–962
DOI 10.1007/s10033-017-0138-9

ORIGINAL ARTICLE

Analytical Compliance Modeling of Serial Flexure-Based Compliant Mechanism Under Arbitrary Applied Load

Li-Ping Wang[1,2] · Yao Jiang[3] · Tie-Min Li[1,2]

Received: 20 December 2015 / Revised: 11 April 2017 / Accepted: 20 April 2017 / Published online: 17 May 2017

Abstract Analytical compliance model is vital to the flexure- based compliant mechanism in its mechanical design and motion control. The matrix is a common and effective approach in the compliance modeling while it is not well developed for the closed-loop serial and parallel compliant mechanisms and is not applicable to the situation when the external loads are applied on the flexure members. Concise and explicit analytical compliance models of the serial flexure-based compliant mechanisms under arbitrary loads are derived by using the matrix method. An equivalent method is proposed to deal with the situation when the external loads are applied on the flexure members. The external loads are transformed to concentrated forces applied on the rigid links, which satisfy the equations of static equilibrium and also guarantee that the deformations at the displacement output point remain unchanged. Then the matrix method can be still adopted for the compliance analysis of the compliant mechanism. Finally, several specific examples and an experimental test are given to verify the effectiveness of the compliance models and the force equivalent method. The research enriches the matrix method and provides concise analytical compliance models for the serial compliant mechanism.

Keywords Compliant mechanism · Compliance modeling · Matrix method

1 Introduction

Compared with conventional mechanisms, flexure-based compliant mechanisms can provide motions without friction, backlash, and wear [1]. Therefore, they are widely used in the applications where high positioning accuracy is required, such as the scanning tunneling microscope, precision positioning stage, X-ray lithography, and wafer alignment in microlithography [2–4].

Flexure-based compliant mechanisms transmit the motions entirely through the deformations of the flexure hinges. Therefore, a concise and accurate compliance model, which establishes the relationship between the deformations and the applied loads, is important and necessary for the optimal design, performance analysis, and accurate motion control of the compliant mechanisms [5]. Many works related to the compliance modeling of the compliant mechanism have been done and the main methods include the pseudo-rigid-body (PRB) model, the Castigliano's theorem, the matrix method, and the finite element model(FEM). The PRB model, initially presented by L L Howell [6], treats the flexure hinge as a revolute joint with an attached torsional spring and provides a simple and intuitive way to estimate the mechanism's compliance. However, this method shows some inaccuracies because the axial and transverse deformations of the

Supported by National Natural Science Foundation of China (Grant No.51675292), National Science and Technology Major Project of China (Grant No. 2015ZX04001002), and Tsinghua University Initiative Scientific Research Program (Grant No. 2014z22068).

✉ Tie-Min Li
litm@tsinghua.edu.cn

[1] Institute of Manufacturing Engineering, Department of Mechanical, Tsinghua University, Beijing 100084, China

[2] Beijing Key Laboratory of Precision/Ultra-Precision Manufacturing Equipments and Control, Tsinghua University, Beijing 100084, China

[3] Institute of Instrument Science and Technology, Department of Precision Instrument, Tsinghua University, Beijing 100084, China

flexure hinges are not taken into consideration. H H Pham, et al. [7], used an extended PRB model, named the PRB-D model, to derived the kinematic model of a flexure-based parallel mechanism. The experimental tests showed that the calculation error of the PRB-D model was only 1/3 compared with the PRB model. P Xu, et al. [8], used the PRB model to establish the compliance model for a variety of beam-based compliant mechanisms with large deformations. S Z Liu, et al. [9], studied the frequency characteristics and sensitivity of the large-deformation compliant mechanism based on a modified PRB model. The Castigliano's theorem derives the compliance model of the compliant mechanism based on the strain energy. N Lobontiu, et al. [10], formulated an analytical compliance model for the planar compliant mechanisms with single-axis flexure hinges based on the Castigliano's displacement theorem. In this research, closed-form equations were produced and a parametric study of the mechanism performance was also carried out. X Jia, et al. [11], obtained the input stiffness model of the active arm of a 3-DOF compliant parallel positioning stage on the basis of the Castigliano's first theorem. The matrix method transforms the local compliance of the flexure members to a global frame for easily obtaining the compliance model of the entire mechanism. Y KOSEKI, et al. [12], applied the matrix method to the kinematic analysis of a translational 3-DOF micro parallel compliant mechanism. H H Pham, et al. [13], used the matrix method to present an analytical stiffness model of a flexure parallel mechanism. S L Xiao, et al. [14], conducted the compliance modeling of a novel compliant micro-parallel positioning stage by means of the matrix method. N Lobontiu [15] proposed a basic three-point compliance matrix method to model the direct and inverse quasi-static response of constrained and over-constrained planar serial compliant mechanisms. The FEM [16–19] has been widely used in the structural mechanics field and is by far the most accurate computational method in calculating the compliance of the compliant mechanism. Since the FEM is a numerical method, the intrinsic characteristic of the compliance of the compliant mechanism cannot be explicitly identified.

From the introductions above, the calculation accuracy of the PRB model is relative low, but it is simple and useful in the early stage of the prototype design and performance analysis of the compliant mechanisms. The FEM, by contrast, is accurate but only appropriate to verify the calculation accuracy of the analytical model or analyze the performance of the compliant mechanism before fabrication. Additionally, compared with the Castigliano's theorem, the matrix method is more simple and effective for the analytical compliance modeling of the compliant mechanism. Therefore, the matrix method is adopted in this article. Though it has been widely used, the matrix method is not well developed in the compliance modeling for the closed-loop serial or parallel compliant mechanism. For example, the matrix method is not well adopted for analyzing the performance of a bridge-type amplifier, including the input stiffness and displacement amplification ratio. Instead, the elastic beam theory together with the kinematic analysis are used to solve this problem [10, 20, 21]. However, the analysis procedure is complex and there are no simple calculation expressions provided for this case. Additionally, the matrix method is not applicable for the compliance analysis when the loads are applied on the flexure members. For instance, when the compliant mechanism is inserted into the dual-stage for accuracy compensation within a long stroke [22], the deformations of the flexure members under inertial forces and gravity cannot be calculated by using the matrix method. Though the Castigliano's theorem can deal with this issue, it involves the partial differential calculation. Therefore, it is meaningful to develop a more effectiveness method for the real-time accuracy compensation control.

This paper focuses on the analytical compliance modeling of the serial flexure-based compliant mechanisms under arbitrary external loads. According to the relative positional relationship between the applied loads and the displacement output point, concise and explicit compliance models of the open- and closed-loops serial compliant mechanisms are derived based on the matrix method. Then an equivalent method is proposed to transform the external loads applied on the flexure members to the concentrated forces applied on the rigid links. The transformation process satisfies the static equilibrium condition and also guarantees that the deformations at the displacement output point remain unchanged. Thus, the matrix method can be still used to analyze the compliance of the compliant mechanisms. Finally, several specific examples are given to illustrate the effectiveness of the proposed method.

2 External Load Applied on Rigid Links

In this section, the compliance modeling of the open- and closed-loops serial compliant mechanisms when the external loads are applied on the rigid links is discussed.

2.1 Compliance Modeling of the Open-Loop Serial Compliant Mechanism

An open-loop serial compliant mechanism, as depicted in Fig. 1, comprises several flexure hinges interconnected with rigid links. One of its ends is fixed and the other end is free. The compliance modeling of the open-loop serial compliant mechanism based on the matrix method has already been investigated [13, 15]. In this section, according to the relative positional relationship between

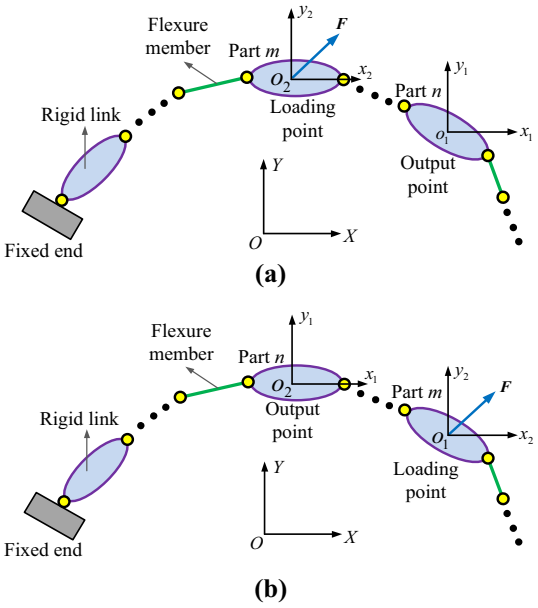

Fig. 1 Open-loop serial flexure-based compliant mechanism

the loading point and the displacement output point, the compliance modeling process is discussed again.

Considering the deformations of the flexure hinges are linear and small, the deformation at a given point of the compliant mechanism can be calculated through the superposition principle. According to the relative position of the applied loads, the compliance modeling of the open-loop serial compliant mechanism is discussed in two difference conditions. Fig. 1(a) shows the loading point is closer to the fixed end than the displacement output point, and Fig. 1(b) shows the displacement output point is closer to the fixed end.

According to Fig. 1(a), only the flexure members between the fixed end and the loading point suffer deformations, and the total deformation at the displacement output point can be obtained as

$$\boldsymbol{\delta}_o = \sum_{i=1}^{m} \boldsymbol{\delta}_i = \sum_{i=1}^{m} \boldsymbol{T}_{id}\, \boldsymbol{\delta}_i^l, \tag{1}$$

where $\boldsymbol{\delta}_i^l$ is the deformation of flexure hinge i represented in its local frame, and $\boldsymbol{T}_{id}$ is the matrix transforming the local deformation $\boldsymbol{\delta}_i^l$ of the flexure hinge to the deformation $\boldsymbol{\delta}_i$ at the displacement output point.

The applied load and deformation of flexure hinge i in its local frame can be expressed as, respectively,

$$\boldsymbol{F}_i = \boldsymbol{T}_{if}\, \boldsymbol{F}, \tag{2}$$

$$\boldsymbol{\delta}_i^l = \boldsymbol{C}_i \boldsymbol{F}_i, \tag{3}$$

where $\boldsymbol{T}_{if}$ is the matrix transforming the external load $\boldsymbol{F}$ to the applied load $\boldsymbol{F}_i$ at flexure hinge i, and $\boldsymbol{C}_i$ is the local compliance matrix of flexure hinge i.

From Eqs. (1)–(3), the deformation at the displacement output point can be written as

$$\boldsymbol{\delta}_o = \sum_{i=1}^{m} \boldsymbol{T}_{id} \boldsymbol{C}_i \boldsymbol{F}_i = \left(\sum_{i=1}^{m} \boldsymbol{T}_{id} \boldsymbol{C}_i \boldsymbol{T}_{if} \right) \boldsymbol{F}, \tag{4}$$

Therefore, the compliance model matrix of the open-loop serial compliant mechanism shown in Fig. 1(a) can be obtained as

$$\boldsymbol{C} = \frac{\partial \boldsymbol{\delta}_0}{\partial \boldsymbol{F}} = \sum_{i=1}^{m} \boldsymbol{T}_{id} \boldsymbol{C}_i \boldsymbol{T}_{if}. \tag{5}$$

Similarly, the compliance matrix of the open-loop serial compliant mechanism shown in Fig. 1(b) can be obtained as

$$\boldsymbol{C} = \sum_{i=1}^{n} \boldsymbol{T}_{id} \boldsymbol{C}_i \boldsymbol{T}_{if}. \tag{6}$$

According to Eqs. (5) and (6), the general compliance model of the open-loop serial compliant mechanism can be expressed as

$$\boldsymbol{C} = \sum_{i=1}^{\min(\mathrm{m},\,\mathrm{n})} \boldsymbol{T}_{id} \boldsymbol{C}_i \boldsymbol{T}_{if} = \boldsymbol{T}_d \boldsymbol{C}^* \boldsymbol{T}_f, \tag{7}$$

where

$$\boldsymbol{T}_d = \begin{pmatrix} \boldsymbol{T}_{1d} & \boldsymbol{T}_{2d} & \cdots & \boldsymbol{T}_{\min(\mathrm{m,n})\mathrm{d}} \end{pmatrix}^{\mathrm{T}},$$

$$\boldsymbol{C}^* = \mathrm{diag}\begin{pmatrix} \boldsymbol{C}_1 & \boldsymbol{C}_2 & \cdots & \boldsymbol{C}_{\min(\mathrm{m,n})} \end{pmatrix},$$

$$\boldsymbol{T}_f = \begin{pmatrix} \boldsymbol{T}_{1f} & \boldsymbol{T}_{2f} & \cdots & \boldsymbol{T}_{\min(\mathrm{m,n})\mathrm{f}} \end{pmatrix}^{\mathrm{T}}.$$

When multiple loads are applied on the mechanism, the deformation at the given displacement output point is calculated as

$$\boldsymbol{\delta}_o = \sum_{j=1}^{k} \left(\left(\sum_{i=1}^{\min(\mathrm{m_j},\,\mathrm{n})} \boldsymbol{T}_{id} \boldsymbol{C}_i \boldsymbol{T}_{if} \right) \boldsymbol{F}_j \right). \tag{8}$$

2.2 Compliance Modeling of the Closed-Loop Serial Compliant Mechanism

Compared with the open-loop serial compliant mechanism, both ends of the closed-loop serial compliant mechanism are fixed, as depicted in Fig. 2.

The closed-loop serial compliant mechanism is over-constrained because its two fixed ends produce more than three unknown reaction forces, which brings difficulty in obtaining its compliance model. Generally, the geometric relationship of the deformations and equations of static equilibrium are provided to deal with this issue. However, this method is relative complex and there are no concise and explicit expressions for the compliance calculation.

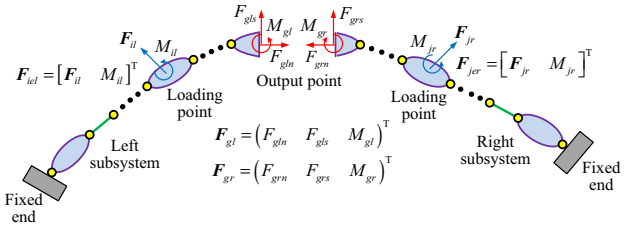

Fig. 2 Closed-loop serial flexure-based compliant mechanism

Due to the over-constrained characteristic of the closed-loop serial compliant mechanism, it is cut out at the displacement output point and the inner forces are applied at the sections, as shown in Fig. 2.

The deformation at the section of the left subsystem can be expressed as

$$\boldsymbol{\delta}_l = \boldsymbol{C}_{gl}\boldsymbol{F}_{gl} + \sum \boldsymbol{C}_{iel}\boldsymbol{F}_{iel}, \tag{9}$$

where $\boldsymbol{C}_{gl}$ is the compliance matrix related to inner force $\boldsymbol{F}_{gl}$ and the displacement output point, and $\boldsymbol{C}_{iel}$ is compliance matrix related to external load $\boldsymbol{F}_{iel}$ and the displacement output point.

The deformation at the section of the right subsystem can be expressed as

$$\boldsymbol{\delta}_r = \boldsymbol{C}_{gr}\boldsymbol{F}_{gr} + \sum \boldsymbol{C}_{jer}\boldsymbol{F}_{jer}, \tag{10}$$

where $\boldsymbol{C}_{gr}$ is the compliance matrix related to inner force $\boldsymbol{F}_{gr}$ and the displacement output point, and $\boldsymbol{C}_{jer}$ is compliance matrix related to external load $\boldsymbol{F}_{jer}$ and the displacement output point.

The deformations and inner forces at the sections satisfy the conditions as

$$\boldsymbol{\delta}_l = \boldsymbol{\delta}_r, \tag{11}$$

$$\boldsymbol{F}_{gl} = -\boldsymbol{F}_{gr} = \boldsymbol{F}_s. \tag{12}$$

Combing Eqs. (9) and (10), the inner force $\boldsymbol{F}_s$ at the section can be obtained as

$$\boldsymbol{F}_s = \left(\boldsymbol{C}_{gl} + \boldsymbol{C}_{gr}\right)^{-1}\left(\sum \boldsymbol{C}_{ier}\boldsymbol{F}_{ier} - \sum \boldsymbol{C}_{jel}\boldsymbol{F}_{jel}\right) \tag{13}$$

Defining $\boldsymbol{B}=\boldsymbol{C}_{gl} + \boldsymbol{C}_{gr}$, and substituting Eq. (13) in Eqs. (8) and (9) leads to, respectively,

$$\boldsymbol{\delta}_l = \sum \left(\boldsymbol{C}_{gl}\boldsymbol{B}^{-1}\boldsymbol{C}_{ier}\right)\boldsymbol{F}_{jer} - \sum \left(\boldsymbol{C}_{gl}\boldsymbol{B}^{-1}\boldsymbol{C}_{iel} - \boldsymbol{C}_{iel}\right)\boldsymbol{F}_{iel}, \tag{14}$$

$$\boldsymbol{\delta}_r = \sum \left(\boldsymbol{C}_{gr}\boldsymbol{B}^{-1}\boldsymbol{C}_{iel}\right)\boldsymbol{F}_{iel} - \sum \left(\boldsymbol{C}_{gl}\boldsymbol{B}^{-1}\boldsymbol{C}_{jer} - \boldsymbol{C}_{jer}\right)\boldsymbol{F}_{jer} \tag{15}$$

According to the relative positional relationship between the loading point and the displacement output point, the compliance model of the closed-loop serial compliant mechanism is discussed as follows.

(1) When the loading point and the displacement output point are coincident, the external load satisfies $\boldsymbol{F}_e=\boldsymbol{F}_{iel}$ and $\boldsymbol{F}_{jer}=\boldsymbol{0}$, or $\boldsymbol{F}_e=\boldsymbol{F}_{jer}$ and $\boldsymbol{F}_{iel}=\boldsymbol{0}$. The deformation at the displacement output point can be expressed as

$$\boldsymbol{\delta} = \left(\boldsymbol{C}_{gl}\boldsymbol{B}^{-1}\boldsymbol{C}_{gr}\right)\boldsymbol{F}_e = \left(\boldsymbol{C}_{gr}\boldsymbol{B}^{-1}\boldsymbol{C}_{gl}\right)\boldsymbol{F}_e. \tag{16}$$

Therefore, the compliance matrix of the mechanism can be written as

$$\boldsymbol{C} = \frac{\partial\boldsymbol{\delta}}{\partial\boldsymbol{F}_e} = \boldsymbol{C}_{gl}\boldsymbol{B}^{-1}\boldsymbol{C}_{gr} = \boldsymbol{C}_{gr}\boldsymbol{B}^{-1}\boldsymbol{C}_{gl}. \tag{17}$$

The stiffness matrix of the mechanism can be obtained as

$$\boldsymbol{K} = \left(\boldsymbol{C}_{gl}\boldsymbol{B}^{-1}\boldsymbol{C}_{gr}\right)^{-1} = \boldsymbol{C}_{gl}^{-1} + \boldsymbol{C}_{gr}^{-1} = \boldsymbol{K}_{gl} + \boldsymbol{K}_{gr}. \tag{18}$$

Eq. (18) indicates that when the loading point and the displacement output point are coincident, the stiffness of the closed-loop serial compliant mechanism can be obtained by adding the stiffness of its subsystems together.

(2) When the external load is applied on the left subsystem, it satisfies $\boldsymbol{F}_e=\boldsymbol{F}_{iel}$ and $\boldsymbol{F}_{jer}=\boldsymbol{0}$. The deformation at the displacement output point can be obtained from Eq. (15) as

$$\boldsymbol{\delta} = \boldsymbol{\delta}_r = \left(\boldsymbol{C}_{gr}\boldsymbol{B}^{-1}\boldsymbol{C}_{el}\right)\boldsymbol{F}_e. \tag{19}$$

Therefore, the compliance matrix of the mechanism can be written as

$$\boldsymbol{C} = \frac{\partial\boldsymbol{\delta}}{\partial\boldsymbol{F}_e} = \boldsymbol{C}_{gr}\boldsymbol{B}^{-1}\boldsymbol{C}_{el}. \tag{20}$$

(3) When the external load is applied on the right subsystem, it satisfies $\boldsymbol{F}_e=\boldsymbol{F}_{jer}$ and $\boldsymbol{F}_{iel}=\boldsymbol{0}$. The deformation at the displacement output point can be obtained from Eq. (14) as

$$\boldsymbol{\delta} = \boldsymbol{\delta}_l = \left(\boldsymbol{C}_{gl}\boldsymbol{B}^{-1}\boldsymbol{C}_{er}\right)\boldsymbol{F}_e. \tag{21}$$

Therefore, the compliance matrix of the mechanism can be given as

$$\boldsymbol{C} = \frac{\partial\boldsymbol{\delta}}{\partial\boldsymbol{F}_e} = \boldsymbol{C}_{gl}\boldsymbol{B}^{-1}\boldsymbol{C}_{er}. \tag{22}$$

According to the discussions, concise and explicit compliance models of the closed-loop serial compliant mechanism can be obtained, which will be helpful in its performance analysis and optimal design.

When multiple loads are applied on the mechanisms, the deformation at the displacement output point is calculated as

$$\boldsymbol{\delta}_o = \sum \left(\boldsymbol{C}_{gr}\boldsymbol{B}_i^{-1}\boldsymbol{C}_{iel}\right)\boldsymbol{F}_{iel} + \sum \left(\boldsymbol{C}_{gl}\boldsymbol{B}_j^{-1}\boldsymbol{C}_{jer}\right)\boldsymbol{F}_{jer}. \tag{23}$$

3 External Loads Applied on the Flexure Members

The relationship between the deformations of the flexure members and the external loads is nonlinear when the loads are applied on the flexure members. The matrix method is only appropriate to the linear problem, and therefore cannot be used to derive the compliance model of the compliant mechanisms in this case. Though the Castigliano's theorem can deal with this issue, it involves the partial differential which leads to a complex calculation process. In this section, an effective equivalent method is proposed to handle with the external loads applied on the flexure members. This method aims at transforming the external loads from the flexure members to the rigid links. The transformation process should satisfy the equations of static equilibrium and guarantee that the deformations at the displacement output point remain unchanged.

Owing to the nonlinear relationship between the deformations and loads applied on the flexure members, it is impossible to transform the external loads to just one concentrated force on the rigid link to satisfy the both two conditions stated above. Therefore, the loads applied on the flexure members are transformed to two concentrated forces applied on the rigid links, as shown in Fig. 3.

The equivalent concentrated forces should satisfy the following conditions as

$$\boldsymbol{\delta}_{iq} = \boldsymbol{\delta}_{if} = \boldsymbol{\delta}_i \ , \ \ \boldsymbol{\delta}_{jq} = \boldsymbol{\delta}_{jf} = \boldsymbol{\delta}_j, \tag{24}$$

$$\boldsymbol{F}_i + \boldsymbol{F}_j = \boldsymbol{q}(x) \ , \ \ \boldsymbol{M}_i + \boldsymbol{M}_j = \boldsymbol{M}_{q(x)}, \tag{25}$$

where $\boldsymbol{\delta}_{iq}$ and $\boldsymbol{\delta}_{if}$ are the deformations at point i caused by original force $\boldsymbol{q}$ and equivalent force $\boldsymbol{F}_i$ respectively, and $\boldsymbol{\delta}_{jq}$ and $\boldsymbol{\delta}_{jf}$ are the deformations at point j caused by original force $\boldsymbol{q}$ and equivalent force $\boldsymbol{F}_j$ respectively.

It is complicated to solve Eqs. (24) and (25) directly. Assuming that forces $\boldsymbol{F}_i$ and $\boldsymbol{F}_j$ satisfy Eq. (24), and we apply forces $-\boldsymbol{F}_i$ and $-\boldsymbol{F}_j$ on the original flexure member at points i and j, respectively. The deformations at the two points caused by the two forces are $-\boldsymbol{\delta}_i$ and $-\boldsymbol{\delta}_j$, respectively. They are superposed on the original deformations caused by force $\boldsymbol{q}$ results in a fixed-fixed flexure member.

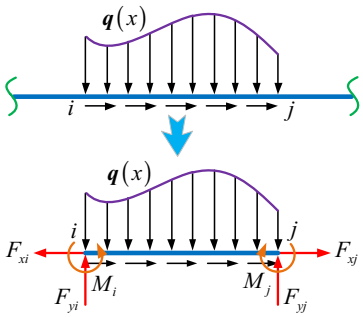

Fig. 3 Equivalent transformation of external loads

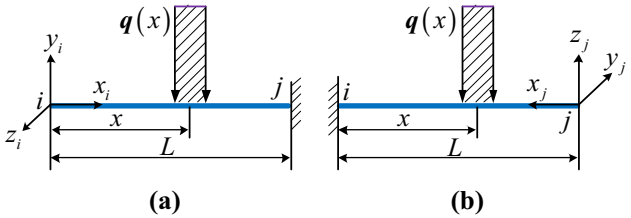

Fig. 4 Calculation of the deformaitons at two points

Therefore, forces $\boldsymbol{F}_i$ and $\boldsymbol{F}_j$ are of course satisfying the equations of static equilibrium represented in Eq. (25).

According to the analysis above, the equivalent forces can be solved only through Eq. (24) and they will satisfy Eq. (25) simultaneously. The deformation at points i or j caused by the original force $\boldsymbol{q}$ can be calculated through the superposition method, as shown in Fig. 4.

According to Fig. 4(a), the deformation at point i caused by the original force $\boldsymbol{q}$ can be obtained as

$$\begin{aligned}\boldsymbol{\delta}_{iq} &= \sum_{k=1}^{\infty}\boldsymbol{\delta}_k^i = \sum_{k=1}^{\infty}\left(\boldsymbol{T}_{kd}^i\boldsymbol{C}_k^i\boldsymbol{T}_{kf}^i\right)\boldsymbol{q}_k \\ &= \int_0^L \left(\boldsymbol{T}_{dx}^i\boldsymbol{C}_x^i\boldsymbol{T}_{fx}^i\right)\boldsymbol{q}(x)\mathrm{d}x.\end{aligned} \tag{26}$$

Similarly, the deformation at point j caused by the original force $\boldsymbol{q}$ can be obtained as

$$\boldsymbol{\delta}_{jq} = \int_0^L \left(\boldsymbol{T}_{dx}^j\boldsymbol{C}_x^j\boldsymbol{T}_{fx}^j\right)\boldsymbol{q}(L-x)\mathrm{d}x. \tag{27}$$

Substituting Eqs. (26) and (27) in Eq. (24) leads to

$$\int_0^L \left(\boldsymbol{T}_{dx}^i\boldsymbol{C}_x^i\boldsymbol{T}_{fx}^i\right)\boldsymbol{q}(x)\mathrm{d}x = \boldsymbol{\delta}_{if} = \boldsymbol{C}_{ig}\boldsymbol{F}_i, \tag{28}$$

$$\int_0^L \left(\boldsymbol{T}_{dx}^j\boldsymbol{C}_x^j\boldsymbol{T}_{fx}^j\right)\boldsymbol{q}(L-x)\mathrm{d}x = \boldsymbol{\delta}_{jf} = \boldsymbol{C}_{jg}\boldsymbol{F}_j, \tag{29}$$

where $\boldsymbol{C}_{ig}$ is the compliance matrix related to equivalent force $\boldsymbol{F}_i$ and point i, and $\boldsymbol{C}_{jg}$ is the compliance matrix related to equivalent force $\boldsymbol{F}_j$ and point j.

The external loads applied on the flexure member can be express as

$$\boldsymbol{q}(x) = \boldsymbol{g}(q)\boldsymbol{f}(x), \tag{30}$$

where $\boldsymbol{g}(q)$ is a coefficient matrix.

Then the equivalent forces $\boldsymbol{F}_i$ and $\boldsymbol{F}_j$ can be obtained as

$$\boldsymbol{F}_i = \boldsymbol{C}_{ig}^{-1}\left(\int_0^L \left(\boldsymbol{T}_{dx}^i \boldsymbol{C}_x^i \boldsymbol{T}_{fx}^i\right)\boldsymbol{f}(x)\,\mathrm{d}x\right)\boldsymbol{g}_i(q) = \left(\boldsymbol{C}_{ig}^{-1}\boldsymbol{C}_{iqx}\right)\boldsymbol{g}_i(q), \tag{31}$$

$$\boldsymbol{F}_j = \boldsymbol{C}_{jg}^{-1}\left(\int_0^L \left(\boldsymbol{T}_{dx}^j \boldsymbol{C}_x^j \boldsymbol{T}_{fx}^j\right)\boldsymbol{f}(L-x)\,\mathrm{d}x\right)\boldsymbol{g}_j(q) = \left(\boldsymbol{C}_{jg}^{-1}\boldsymbol{C}_{jqx}\right)\boldsymbol{g}_j(q). \tag{32}$$

It can be verified that the equivalent forces satisfy Eqs. (24) and (25). Once the external loads are transformed to the concentrated forces applied on the rigid links, the matrix method can be still adopted to analyze the compliance of the compliant mechanisms by using the models derived in section 2.

4 Applications in the Analysis of Serial Flexure-Based Compliant Mechanism

Several specific examples are given in this part to illustrate the effectiveness and validity of the compliance modeling of serial flexure-based compliant mechanisms and the force equivalent method.

4.1 Compliance Analysis of an Open-Loop Serial Compliant Mechanism

A complex open-loop serial compliant mechanism was designed, as shown in Fig. 5. Circular flexure hinge was selected as the flexure member. The derived models based on the matrix method were used to analyze its compliance related to the given loads and displacement output points, as shown in Fig. 6. The finite element analysis (FEA) result was used as a benchmark to verify the accuracy of the analytical model.

The dimensions of the open-loop compliant mechanism were shown in Fig. 5. The geometric parameters of the circular flexure hinge were shown in Fig. 7, and their

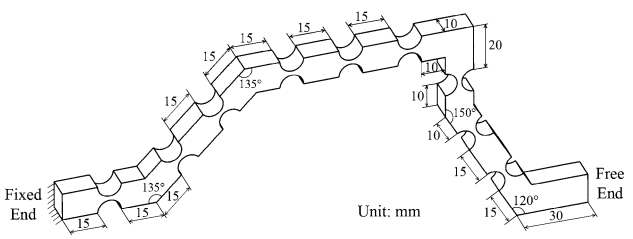

Fig. 5 Open-loop serial compliant mechanism

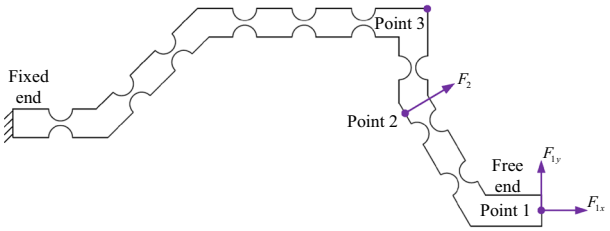

Fig. 6 External loads and displacement output points

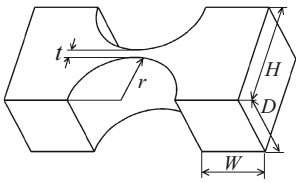

Fig. 7 Circular flexure hinge and its dimensions

Table 1 Calculation errors of each compliance component %

Compliance component	Thickness t / mm		
	1 mm	3 mm	5 mm
$C_{1x\text{-}F1x}$	–3.83	0.04	2.96
$C_{1y\text{-}F1x}$	–1.64	2.16	5.10
$C_{1x\text{-}F1y}$	–1.64	2.16	5.10
$C_{1y\text{-}F1y}$	1.74	5.53	9.15

dimensions were given as r = 5 mm, W = 5 mm, t = 1 mm, 3 mm, and 5 mm, respectively.

The motion of this compliant mechanism is mainly provided by the deformations of all the circular flexure hinges. Therefore, an accurate compliance equation of the flexure hinge is important for obtaining a precise compliance model of the entire mechanism. An empirical compliance equation[23] for the circular flexure hinge was adopted in this paper.

Firstly, point 1 was selected as both the loading point and the displacement output point. Utilizing the FEA result as the benchmark, the calculating errors of each compliance components of the mechanism were given in Table 1.

The results show that the analytical model has relative high calculation accuracy. One may see that the calculation errors increase as the minimum thickness t of the flexure hinge grows. The possible reason is that the rigid links are not absolute rigid and also undergoes elastic deformations. When the circular flexure hinges grow thicker, the relative proportion of the deformations of the rigid links increases. Considering the compliance of the rigid links, the calculation errors of each compliance components of the mechanism were given in Table 2. It shows that the calculation accuracies are obviously improved, especially when t = 3 mm and 5 mm.

Table 2 Calculation errors of each compliance Component %

Compliance component	Thickness t / mm		
	1 mm	3 mm	5 mm
$C_{1x\text{-}F1x}$	–4.14	–2.51	–2.37
$C_{1y\text{-}F1x}$	–1.96	–0.35	–0.08
$C_{1x\text{-}F1y}$	–1.96	–0.35	–0.08
$C_{1y\text{-}F1y}$	1.36	2.62	3.18

Table 3 Compliance of the mechanism calculated through the FEA μm / N

Compliance component	Thickness t / mm		
	1 mm	3 mm	5 mm
$C_{3x\text{-}F2}$	–117.07	–8.779	–2.753
$C_{3y\text{-}F2}$	526.60	38.692	11.905

Table 4 Compliance of the mechanism calculated through the analytical model μm / N

Compliance component	Thickness t / mm		
	1 mm	3 mm	5 mm
$C_{3x\text{-}F2}$	–113.45	–8.391	–2.627
$C_{3y\text{-}F2}$	518.65	37.526	11.519

Secondly, the external load was applied at point 2 and vertical to the surface, and point 3 was selected as the displacement output point. The compliance of the mechanism calculated through the FEA and the analytical model were given in Tables 3 and 4, respectively.

The simulation analyses show that the matrix method is applicable to the compliance modeling of the open-loop serial compliant mechanism related to any given output points and external loads applied on the rigid links. Additionally, the compliance of the rigid links cannot be neglected when the flexure hinges are relative thick and the length of the open-loop serial chain is long.

4.2 Transformation of the External Loads Applied on Flexure Members

Fig. 8 shows a serial compliant chain composed of rectangular flexure members and rigid links. The external loads $q_1(x)$ and $q_2(x)$ were applied on the flexure members. The force equivalent method was used to transform the external loads from the flexure members to the rigid links.

The equivalent transformation of external load $q_1(x)$ was first discussed. It was transformed to two concentrated forces applied at points 1 and 2. The local coordinate

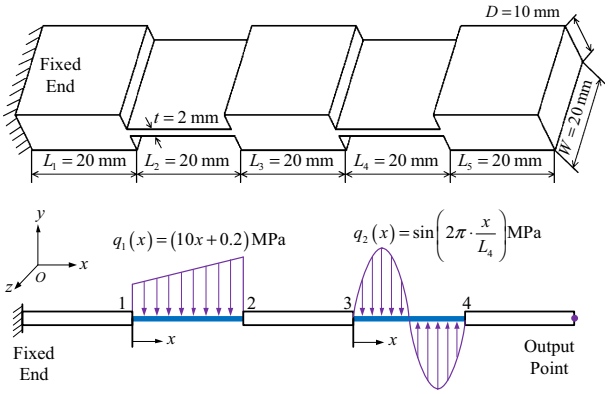

Fig. 8 External loads applied on the flexure membmers

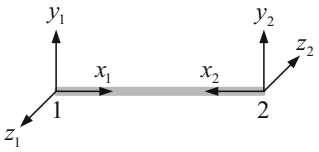

Fig. 9 Local coordiante frames at points 1 and 2

frames at points 1 and 2 were established, as shown in Fig. 9.

According to Eqs. (31) and (32), equivalent forces $\boldsymbol{F}_1$ and $\boldsymbol{F}_2$ were obtained in each local coordinate frame as, respectively,

$$\boldsymbol{F}_1' = \boldsymbol{C}_{1g}^{-1}\left(\int_0^{L_2}\left(\boldsymbol{T}_{dx}^1\boldsymbol{C}_x^1\boldsymbol{T}_{fx}^1\right)\boldsymbol{f}_1(x)\,\mathrm{d}x\right)\boldsymbol{g}(q_1), \tag{33}$$

$$\boldsymbol{F}_2' = \boldsymbol{C}_{2g}^{-1}\left(\int_0^{L_2}\left(\boldsymbol{T}_{dx}^2\boldsymbol{C}_x^2\boldsymbol{T}_{fx}^2\right)\boldsymbol{f}_1(L_2-x)\,\mathrm{d}x\right)\boldsymbol{g}(q_1). \tag{34}$$

where

$$\boldsymbol{q}_1(x) = \boldsymbol{f}_{1\_1}(x)\boldsymbol{g}_{1\_1}(q_1) + \boldsymbol{f}_{1\_2}(x)\boldsymbol{g}_{1\_2}(q_1) = \begin{pmatrix}0&0&0\\0&x&0\\0&0&0\end{pmatrix}\begin{pmatrix}0\\10W\\0\end{pmatrix} + \begin{pmatrix}0&0&0\\0&1&0\\0&0&0\end{pmatrix}\begin{pmatrix}0\\0.2W\\0\end{pmatrix},$$

$$\boldsymbol{C}_{1g} = \boldsymbol{C}_{2g} = \begin{pmatrix}\frac{L_2}{EDt} & 0 & 0\\ 0 & \frac{4L_2^3}{EDt^3} + \alpha\frac{E}{G}\cdot\frac{L_2}{EDt} & -\frac{6L_2^2}{EDt^3}\\ 0 & -\frac{6L_2^2}{EDt^3} & \frac{12L_2}{EDt^3}\end{pmatrix},$$

$$\boldsymbol{C}_x^1 = \boldsymbol{C}_x^2 = \begin{pmatrix}\frac{L_2-x}{EDt} & 0 & 0\\ 0 & \frac{4(L_2-x)^3}{EDt^3} + \alpha\frac{E}{G}\cdot\frac{L_2-x}{EDt} & -\frac{6(L_2-x)^2}{EDt^3}\\ 0 & -\frac{6(L_2-x)^2}{EDt^3} & \frac{12(L_2-x)}{EDt^3}\end{pmatrix},$$

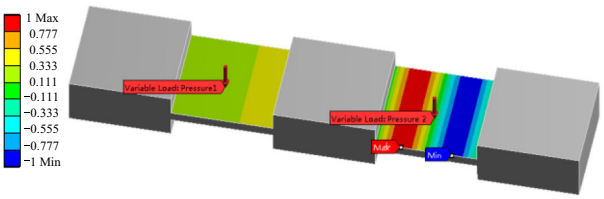

(a) External loads applied on the flexure members

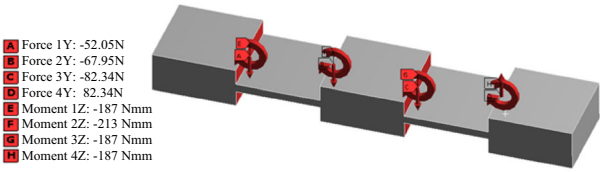

(b) Equivalent concentrated forces applied on the rigid links

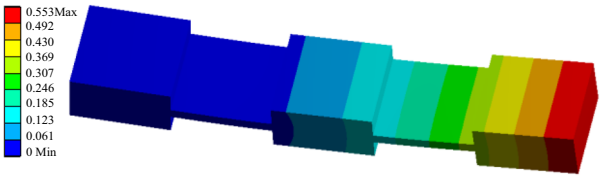

(c) Deformation analysis

Fig. 10 Equivalent transformation method verified by the FEA software

$$\boldsymbol{T}_{dx}^{1} = \boldsymbol{T}_{dx}^{2} = \begin{pmatrix} 1 & 0 & 0 \\ 0 & 1 & -x \\ 0 & 0 & 1 \end{pmatrix}, \quad \boldsymbol{T}_{fx}^{1} = \boldsymbol{T}_{fx}^{1} = \begin{pmatrix} 1 & 0 & 0 \\ 0 & 1 & 0 \\ 0 & 0 & 1 \end{pmatrix}.$$

The equivalent forces $\boldsymbol{F}_1$ and $\boldsymbol{F}_2$ were calculated in the global coordinate frame as $\boldsymbol{F}_1$ = (0–52.05 N –0.187 Nm)$^{\mathrm{T}}$ and $\boldsymbol{F}_2$ = (0–67.95 N –0.213 Nm)$^{\mathrm{T}}$.

Similarly, external load $q_2(x)$ was transformed to two equivalent forces applied at points 3 and 4 respectively as $\boldsymbol{F}_3$ = (0–82.34 N –0.187 Nm)$^{\mathrm{T}}$ and $\boldsymbol{F}_2$ = (0 82.34 N –0.187 Nm)$^{\mathrm{T}}$.

The FEA software was used to calculate the deformation at the output point caused by all the external loads and the equivalent loads, as shown in Fig. 10. The results were $\boldsymbol{\delta}$ = (0 0.541 0)$^{\mathrm{T}}$ mm and $\boldsymbol{\delta}_e$ = (0 0.551 0)$^{\mathrm{T}}$ mm, respectively.

The results show that the deformations at the given displacement output point caused by the original external loads and the equivalent forces are almost the same. Additionally, it can be verified that the equivalent forces satisfy the equations of static equilibrium. The analysis proves the effectiveness and validity of the proposed equivalent transformation method for handling the external loads applied on the flexure members.

Macro-micro system is desirable in the applications where the merits of long stroke motion and high accuracy

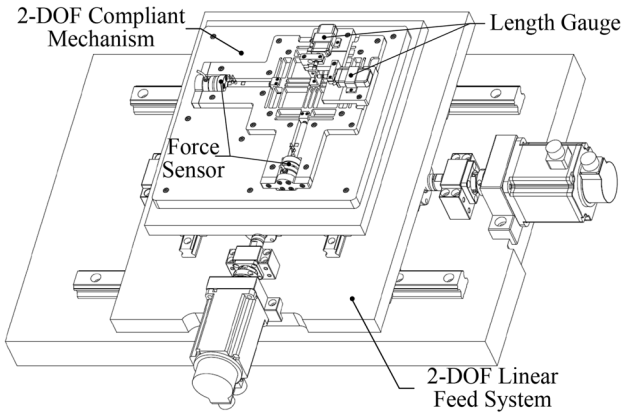

Fig. 11 Macor-micro manipulator

are required. Figure 11 shows a macro-micro manipulator, which is composed of a 2-DOF linear feed system actuated by servo motors and a 2-DOF compliant mechanism actuated by piezoelectric actuators. The linear feed system provides a large stroke motion with a coarse accuracy due to the inevitable clearance, friction, and wear. To achieve high motion accuracy, a compliant mechanism is mounted on the moving platform of the linear feed system to compensate its motion error. However, the flexure members of the compliant mechanism will suffer inertial forces during the acceleration and deceleration stages of the moving platform of the linear feed system. The effect of the inertial forces on the motion accuracy of the compliant mechanism should be considered. The proposed equivalent transformation method can be used to deal with this problem. Then a real-time accuracy compensation control strategy can be carried out with the help of the high precision length gauges. This will be discussed in detail in our future work.

4.3 Amplification Ratio Analysis of a Displacement Amplifier

To illustrate the effectiveness of the derived compliance model of the closed-loop serial compliant mechanism, a bridge-type compliant displacement amplifier was adopted as the object of study. This amplifier has a compact structure and is mainly used for amplifying the displacement of the piezoelectric actuator. Its structure and geometric parameters were given in Fig. 12. Circular flexure hinges[24, 25] were adopted due to their high precision in motion. The initial dimensions of the amplifier were given as C = 30 mm, L = 35 mm, P = 25 mm, E = 12.5 mm, D = 10 mm, and θ= 5 °. The dimensions of the circular flexure hinges were given as r = 5 mm, t = 1 mm, and W = 5 mm.

The boundary condition, applied loads, and displacement output point of this amplifier were shown in Fig. 13.

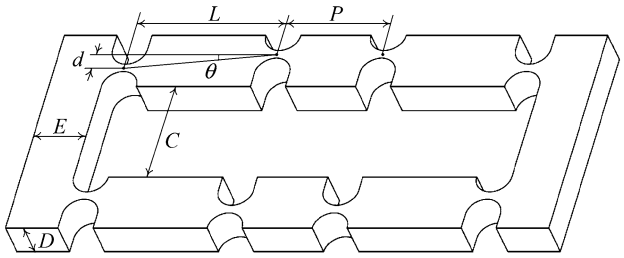

Fig. 12 Schematic diagram of a bridge-type compliant displacement amplifer

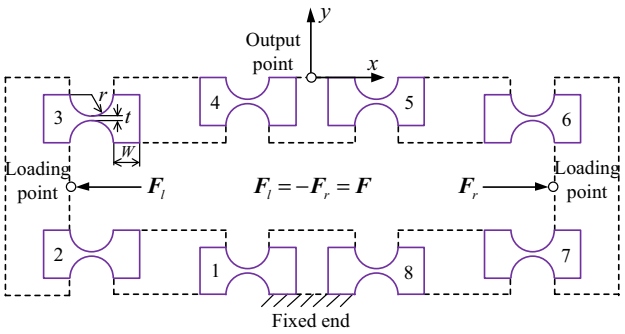

Fig. 13 Boundary conditions, applied loads, and displacement output point

The displacement amplification ratio is the most important performance index for this amplifier, and it is defined as

$$R_{\text{amp}} = \left|\frac{\delta_{oy}}{2\delta_{ix}}\right|, \tag{35}$$

where δ_{oy} is the deformation at the displacement output point, and δ_{ix} is the deformation at any loading point.

To obtain the deformation at the displacement output point, the mechanism was cut out at this point, as shown in Fig. 14. According to Eq. (23), the output displacement was calculated as

$$\begin{aligned}\boldsymbol{\delta}_o = \left(\boldsymbol{C}_{gr\_o}\boldsymbol{B}_{1\_o}^{-1}\boldsymbol{C}_{el\_o}\right)\boldsymbol{F}_l + \left(\boldsymbol{C}_{gl\_o}\boldsymbol{B}_{2\_o}^{-1}\boldsymbol{C}_{er\_o}\right)\boldsymbol{F}_r = \\ \left(\left(\boldsymbol{C}_{gr\_o}\boldsymbol{B}_o^{-1}\boldsymbol{C}_{el\_o}\right) - \left(\boldsymbol{C}_{gl\_o}\boldsymbol{B}_o^{-1}\boldsymbol{C}_{er\_o}\right)\right)\boldsymbol{F},\end{aligned} \tag{36}$$

where $\boldsymbol{C}_{gl\_o} = \sum_{j=1}^{4}\boldsymbol{T}_{jd}^{o}\boldsymbol{C}\boldsymbol{T}_{jf}^{o}$, $\boldsymbol{C}_{gr\_o} = \sum_{j=5}^{8}\boldsymbol{T}_{jd}^{o}\boldsymbol{C}\boldsymbol{T}_{jf}^{o}$, $\boldsymbol{C}_{el\_0} = \sum_{j=1}^{2}\boldsymbol{T}_{jd}^{o}\boldsymbol{C}\boldsymbol{T}_{jf}^{i}$, $\boldsymbol{C}_{er\_o} = \sum_{j=7}^{8}\boldsymbol{T}_{jd}^{o}\boldsymbol{C}\boldsymbol{T}_{jf}^{i}$, $\boldsymbol{B}_o = \left(\boldsymbol{C}_{gl\_o} + \boldsymbol{C}_{gr\_o}\right)$.

To obtain the deformation at the loading point, the mechanism was cut out at the loading point, as shown in Fig. 15. The input displacement was calculated as

$$\begin{aligned}\boldsymbol{\delta}_i = \left(\boldsymbol{C}_{gr\_i}\boldsymbol{B}_{1\_i}^{-1}\boldsymbol{C}_{el\_i}\right)\boldsymbol{F}_l + \left(\boldsymbol{C}_{gl\_i}\boldsymbol{B}_{2\_i}^{-1}\boldsymbol{C}_{er\_i}\right)\boldsymbol{F}_r = \\ \left(\left(\boldsymbol{C}_{gr\_i}\boldsymbol{B}_i^{-1}\boldsymbol{C}_{el\_i}\right) - \left(\boldsymbol{C}_{gl\_i}\boldsymbol{B}_i^{-1}\boldsymbol{C}_{er\_i}\right)\right)\boldsymbol{F},\end{aligned} \tag{37}$$

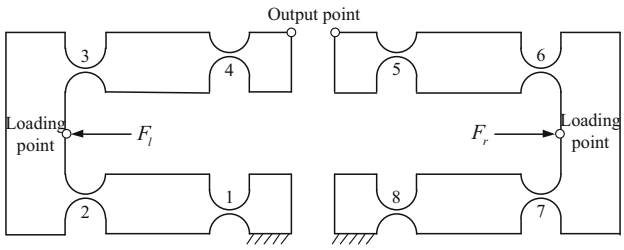

Fig. 14 Subsystems division for calucating output displacement

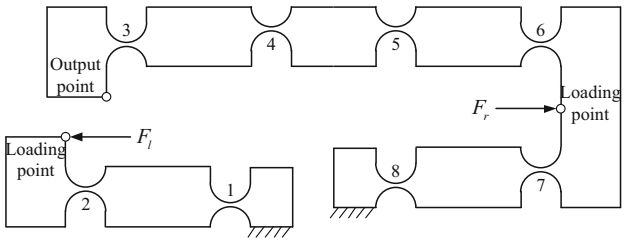

Fig. 15 Subsystems division for calucating input displacement

where $\boldsymbol{C}_{gl\_i} = \sum_{j=1}^{2}\boldsymbol{T}_{jd}^{o}\boldsymbol{C}\boldsymbol{T}_{jf}^{o}$, $\boldsymbol{C}_{gr\_i} = \sum_{j=3}^{8}\boldsymbol{T}_{jd}^{o}\boldsymbol{C}\boldsymbol{T}_{jf}^{o}$, $\boldsymbol{C}_{el\_i} = \sum_{j=1}^{2}\boldsymbol{T}_{jd}^{o}\boldsymbol{C}\boldsymbol{T}_{jf}^{i}$, $\boldsymbol{C}_{er\_i} = \sum_{j=7}^{8}\boldsymbol{T}_{jd}^{o}\boldsymbol{C}\boldsymbol{T}_{jf}^{i}$, $\boldsymbol{B}_i = \left(\boldsymbol{C}_{gl\_i} + \boldsymbol{C}_{gr\_i}\right)$.

Then the displacement amplification ratio of this amplifier was obtained as

$$R_{\text{amp}} = \left|\frac{\left[\left(\boldsymbol{C}_{gr\_o}\boldsymbol{B}_o^{-1}\boldsymbol{C}_{el\_o}\right) - \left(\boldsymbol{C}_{gl\_o}\boldsymbol{B}_o^{-1}\boldsymbol{C}_{er\_o}\right)\right]\boldsymbol{e}_y}{2\cdot\left[\left(\boldsymbol{C}_{gr\_i}\boldsymbol{B}_i^{-1}\boldsymbol{C}_{el\_i}\right) - \left(\boldsymbol{C}_{gl\_i}\boldsymbol{B}_i^{-1}\boldsymbol{C}_{er\_i}\right)\right]\boldsymbol{e}_x}\right|. \tag{38}$$

From Eq. (38), one may see that the displacement amplification ratio is determined by the geometric parameters of the amplifier and the flexure hinges. The influences of the main geometric parameters on the amplification ratio were investigated and shown in Fig. 16. Analytical model I did not consider the compliance of the rigid links, and analytical model II considered the influence of the compliance of the rigid links.

From Fig. 16, the following conclusions can be drawn:

(1) The displacement amplification ratio decreases as geometric parameters P, C, and t increase, and increases as geometric parameter L increases.

(2) The displacement amplification ratio at first increases shapely when angleθincreases, whereas decreases when angleθincreases continuously.

(3) The displacement amplification ratio calculated by the analytical model without considering the compliance of the rigid links is always larger.

(4) The comparisons of the analytical and FEA results demonstrate the accuracy and effectiveness of the derived

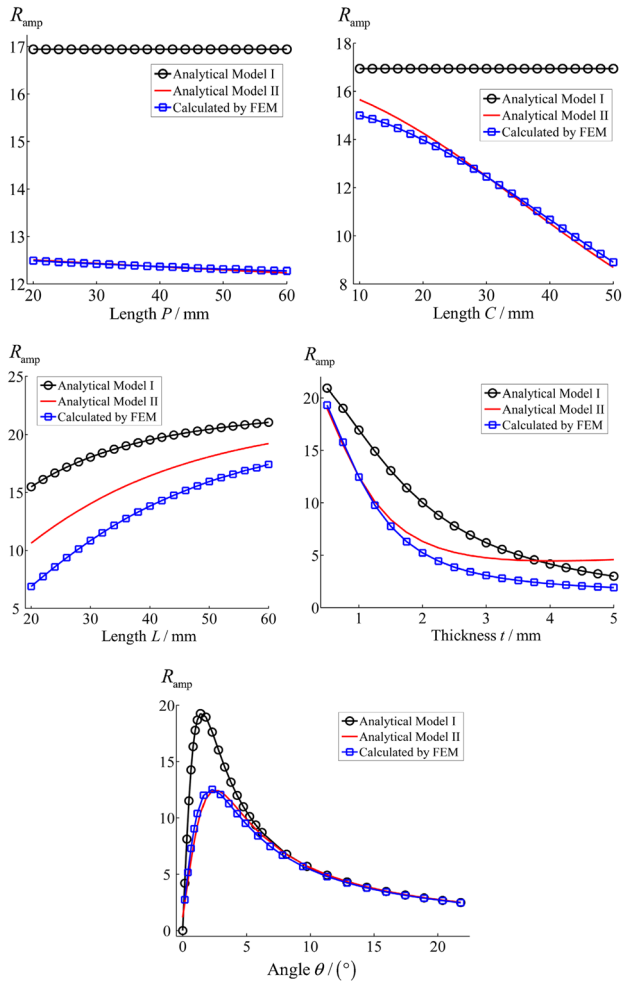

Fig. 16 Influences of the geometric parameters on the displacement ampification ratio of the amplifier

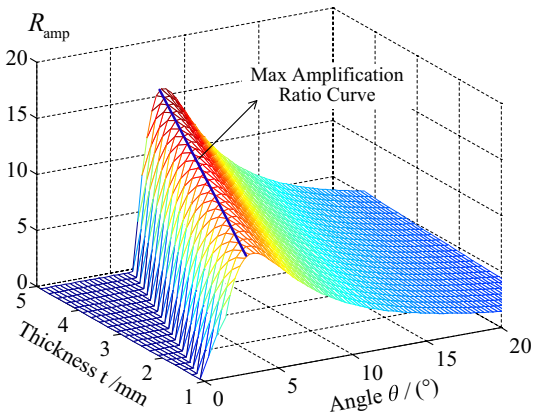

Fig. 17 Influence of angle θ and thickness t on the displacement amplification ratio

compliance model of the closed-loop compliant mechanism. Additionally, the concise expression form will be helpful to the further performance analysis and optimal design.

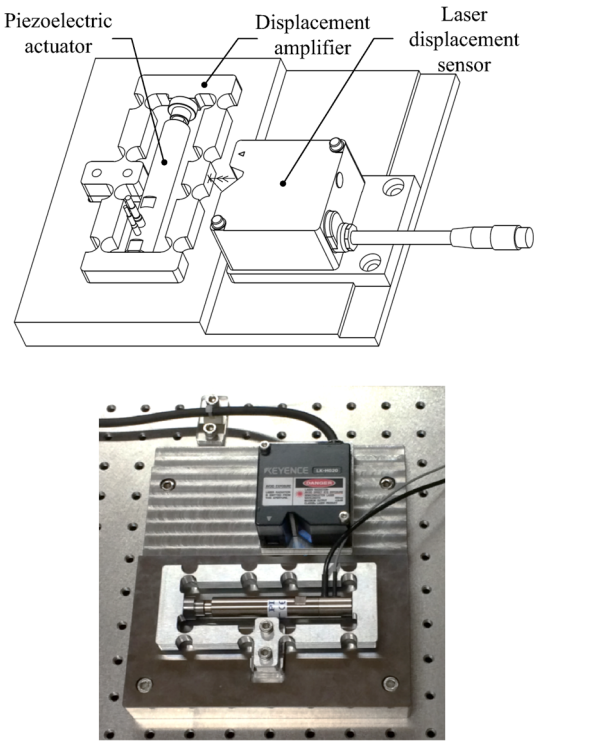

Fig. 18 Experiment table used for testing the displacement amplification ratio of the amplifier

The results show that angle$\theta$and thickness t have great influences on the displacement amplification ratio, and their influences were given in Fig. 17. One may see that there exists a max amplification ratio curve, and it can be used to guide the geometric parametric optimization to obtain a large amplification ratio.

Therefore, small geometric parameters P, C, and t, large geometric parameter L, and optimized angleθcan be chosen to improve the displacement amplification ratio of the amplifier. The optimization of the amplification ratio can be realized based on Eq. (38) with the consideration of other factors, such as the size dimension, input/output compliance, and frequency.

To further verify the accuracy of the analytical model, an experimental table was constructed to test the displacement amplification ratio of the amplifier, as depicted in Fig. 18. The material was steel with a Young's modulus of 210 GPa, and a Poisson's ratio of 0.3. The amplifier was fabricated through the milling process with an accuracy of ±5 μm. A pre-tight piezoelectric actuator (P-843.40 from PI) was adopted to drive the mechanism, and its motion stroke was 60 μm. The input displacement was measured by the integrated feedback sensor of the actuator, and the output displacement was measured by the laser displacement sensor (LK-H025 from Keyence) with a linearity of ±0.02% over a measuring range of 6 mm.

Table 5 Displacement amplification ratios of the amplifiers

Geometric parameters					Amplification ratio	
C / mm	P / mm	L / mm	d / mm	t / mm	Analytical result	Experimental result
30	25	35	1.5	1	12.46	11.92
30	25	35	4.5	1	7.38	7.14

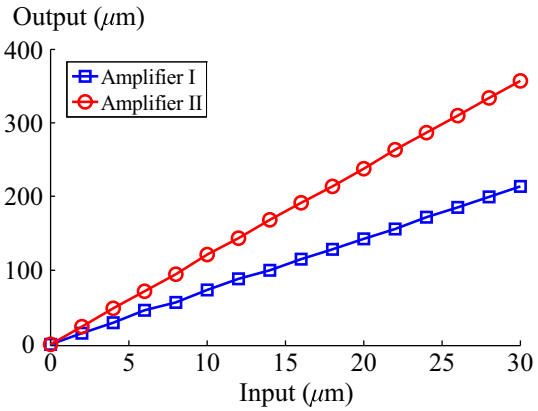

Fig. 19 Input and output displacement measurement results of the two amplifiers

Two amplifiers were used for the experimental tests and their geometric parameters were given in Table 5. The input and output displacements of the two amplifiers were recorded simultaneously when the displacement of the actuator was increased from 0 μm to 30 μm, and the measuring results were shown in Fig. 19. The tested displacement amplification ratios were calculated by using the least square method and the results were shown in Table 5. It shows that the analytical model has relative high calculation accuracy.

5 Conclusions

(1) According to the relative positional relationship between the applied loads and the given displacement output point, the concise and explicit compliance models of the open- and closed-loop serial compliant mechanisms are derived based on the matrix method.

(2) An equivalent method is proposed to transform the external loads applied on the flexure members to the concentrated forces applied on the rigid links. Therefore, the matrix method can be still used to analyze the deformations and compliance of the compliant mechanism.

(3) Several specific simulation analyses and an experimental test are carried out. The results verify the effectiveness and accuracy of the derived compliance models and the force equivalent transformation method.

References

1. Y Tian, B Shirinzadeh, D Zhan, et al. Three flexure hinges for compliant mechanism designs based on dimensionless graph analysis. *Precision Engineering*, 2010, 34(1): 92–100.
2. G Schitter, P J Thurner, P K Hansma. Design and input-shaping control of a novel scanner for high-speed atomic force microscopy. *Mechatronics*, 2006, 18(5–6): 282–288.
3. J A Miller, R Hocken, S T Simith, et al. X-ray calibrated tunneling system utilizing a dimensionally scale nanometer positioner. *Precision Engineering*, 1996, 18(2–3): 95–102.
4. K B Choi, J J Lee. Passive compliant wafer stage for single-step nano-imprint lithography. *Review of Scientific Instruments*, 2005, 76(7): 75106–1–6.
5. H J Su, H L Shi, J J Yu. A symbolic formulation for analytical compliance analysis and synthesis of flexure mechanisms. *Journal of Mechanical Design*, 2012, 134(5):051009–1–9.
6. L L Howell. *Compliant mechanisms*. *New York: Wiley*, 2001.
7. H H Pham, I M Chen, H C Yeh. Micro-motion selective- actuation XYZ flexure parallel mechanism: design and modeling. *Journal of Micromechatronics*, 2005, 3(1): 51–73.
8. P Xu, J J Yu, G H Zhong, et al. An effective pseudo-rigid-body method for beam-based compliant mechanisms. *Precision Engineering*, 2010, 34(3): 634–639.
9. S Z Liu, J S Dai, A M Li, et al. Analysis of frequency characteristics and sensitivity of compliant mechanisms. *Chinese Journal of Mechanical Engineering*, 2016, 29(4): 680–693.
10. N Lbontiu, E Garcia. Analytical model of displacement amplification and stiffness optimization for a class of flexure-based compliant mechanisms. *Computer and Structure*, 2003, 81(32): 2797–2810.
11. X Jia, J Liu, Y Tian, et al. Stiffness analysis of a compliant precision positioning stage. *Robotica*, 2012, 30: 925–939.
12. Y Koseki, T Tanikawa, N Koyachi, et al. Kinematic analysis of a translational 3-dof micro-parallel mechanism using the matrix method. *Advanced Robotics*, 2002, 16(3): 251–264.
13. H H Pham, I M Chen. Stiffness modeling of flexure parallel mechanism. *Precision Engineering*, 2005, 29(4): 467–478.
14. S L Xiao, Y M Li. Development of a large working range flexure-based 3-dof micro-parallel manipulator driven by electromagnetic actuators//*IEEE International Conference on Robotics and Automation*, Karlsruhe, Germany, May 6-10, 2013: 4506–4511.
15. [15]N Lobontiu. Compliance-based matrix method for modeling the quasi-static response of planar serial flexure-hinge mechanisms. *Precision Engineering*, 2014, 38(3): 639–650.
16. [16]S L Zhang, E D Fasse. A finite-element-based method to

determine the spatial stiffness properties of a notch hinge. *Journal of Mechanical Design*, 2001, 123(1): 335–345.
17. [17]H Wang, X M Zhang. Input coupling analysis and optimal design of a 3-DOF compliant micro-positioning stage. *Mechanism and Machine Theory*, 2008, 43(4): 400–410.
18. [18]Y M Li, S L Xiao, L Q Xi, et al. Design, modeling, control and experiment for a 2-DOF compliant micro-motion stage. *Journal of Precision Engineering Manufacturing*, 2014, 15(4): 735–744.
19. [19]Y Yan, H B Wang, Q Li, et al. Finite element simulation of flexible roll forming with supplemented material data and the experimental verification. *Chinese Journal of Mechanical Engineering*, 2016, 29(2): 342–350.
20. [20]H W Ma, S M Yao, L Q Wang, et al. Analysis of the displacement amplification ratio of bridge-type flexure hinge. *Sensor Actuators A: Physics*, 2006, 132(2): 730–736.
21. Q S Xu, Y M Li. Analytical modeling, optimization and testing of a compound bridge-type compliant displacement amplifier. *Mechanism and Machine Theory*, 2011, 46(2): 183–200.
22. [22]R F Fung, Y L Hsu, M S Huang. System identification of a dual-stage XY precision positioning table. *Precision Engineering*, 2009, 33(1): 71–80.
23. T M Li, J L Zhang, Y Jiang. Derivation of empirical compliance equations for circular flexure hinge considering the effect of stress concentration. *Journal of Precision Engineering Manufacturing*, 2015, 16(8): 1735–1743.
24. Y F Wu, Z Y Zhou. Design calculations for flexure hinges. *Review of Scientific Instruments*, 2002, 73(8): 3101–3106.
25. N Lobontiu. *Compliance mechanism: design of flexure hinges*. New York: CPC Press, 2003.

Li-Ping Wang, born in 1967, is currently a professor and a PhD candidate supervisor at *Manufacturing Engineering Institute*, *Department of Mechanical Engineering*, *Tsinghua University, China*. He received his PhD degree from *Jilin University of Technology*, *China*, in 1997. His research interests include advanced equipment and parallel kinematic machine. E-mail: lpwang@tsinghua.edu.cn.

Yao Jiang, born in 1989, is currently a postdoctor at *Institute of Instrument Science and Technology*, *Department of Precision Instrument*, *Tsinghua University*, *China.* He received his PhD degree from *Tsinghua University*, *China*, in 2016. His research interests include dynamic and control of redundant kinematic parallel machine, and compliant mechanism. E-mail: jiangyaonju@126.com.

Tie-Min Li, born in 1971, is currently an associate research fellow at *Manufacturing Engineering Institute*, *Department of Mechanical Engineering*, *Tsinghua University*, *China*. He received his PhD degree from *Tsinghua University*, *China*, in 2000. His interests include robotics and parallel kinematic machine. E-mail: litm@tsinghua.edu.cn